Application of phase contrast imaging atomic force microscopy to tribofilms on DLC coatings

H.-S. Ahn [a,*], S.A. Chizhik [b], A.M. Dubravin [b], V.P. Kazachenko [c], V.V. Popov [c]

[a] *Tribology Research Center, Korea Institute of Science and Technology, 39-1 Hawolgok-dong, Songbuk-gu, Seoul 136-791, South Korea*
[b] *Metal Polymer Research Institute, 32a Kirov St. Gomel, Belarus*
[c] *Belarusian State Transportation University, 34 Kirov St. Gomel, Belarus*

Abstract

Tribofilms formed in the rubbing surfaces are closely related to wear mechanisms and steady-state friction in sliding contacts. However, their small thickness, inhomogeneity and discontinuity are the factors that hinder the evaluation of their micromechanical properties. The phase contrast images in tapping mode atomic force microscopy allow an estimation of inhomogeneity in micromechanical properties of the sample surfaces. The purpose of this investigation is to examine how the phase contrast images contribute to the characterization of thin tribofilms. Surfaces of diamond-like-carbon (DLC) coatings before and after friction contact against a steel ball slider were investigated in this study. The chemical characteristics of the worn surfaces were studied by micro-Raman spectroscopy, Auger electron spectroscopy (AES) and secondary ion mass spectroscopy (SIMS) and these results were discussed in association with the phase contrast images. A three-dimensional simulation of the real contact area was also conducted and the pressure distribution obtained by this simulation was compared with the phase contrast image obtained at the same area.

The phase contrast images revealed a significant inhomogeneity of the worn surfaces. Thin tribofilms were formed at the real contact regions and their thickness increased at the locations experiencing higher contact pressure. The tribofilms that represented as darker grey scale values indicated that they were less stiff than the initial DLC coating. The comparison of the phase contrast images with the results of micro-Raman, AES and SIMS analyses led to a speculation that the tribolfilms, composed almost of carbon element, may be graphite films or films mainly possessing graphitic property. The phase contrast imaging in atomic force microscopy showed promise as an effective tool for better understanding micromechanical properties of worn surfaces and wear mechanisms. © 2001 Elsevier Science B.V. All rights reserved.

Keywords: Atomic force microscopy; Phase contrast image; Stiffness; DLC coating; Tribofilm

1. Introduction

The atomic force microscopy shows promise to provide a fundamental understanding of tribological phenomena at micro- and nanoscale [1]. To achieve a measurement of ultra-low forces at high resolution down to a molecular scale, and without significant influences of tip-sample contact adhesion and capillary effects by adsorbed water layer, the atomic force microscope (AFM) may be used with dynamic mode of the cantilever. This approach is realized by using a tapping mode of scanning [2]. Although the tapping mode is usually used with cantilevers having rather high stiffness (10–100 N/m), plastic deformation of sample materials is minimal since the duration of contact is not enough to cause plastic deformation, the frequency of oscillation of the probe

is usually higher than 100 kHz and the contact time between the probe and the sample is <1 μs at a scan speed of 1 μm/s [3]. However, even with such a short contact time, a variation of important parameters of oscillation, such as amplitude, frequency and phase shift occurs.

The phase contrast image is constructed by monitoring the phase shift during the scan. Since, the phase shift is highly sensitive to tip–sample force interaction, the phase contrast images contain information related to micromechanical properties of the sample materials (elastic modulus, viscoelasticity (damping)) and adhesion generated between the probe tip and the sample surface (surface energy, capillary forces) [4–7]. Recent works conducted by several investigators showed that the phase contrast images were highly effective for estimating structural inhomogeneity of materials [8–12]. It was reported that, in cases where the tip–sample interaction is in a strongly repulsive regime and the effect of damping is small, the phase shift

---

increases when the probe moves from a less stiff material to a stiffer one [6,13,14]. Our previous experimental works also demonstrated that the influence of modulus of elasticity on the phase shift was dominant for hard materials [15,16]. We analyzed the phase contrast images and force-distance curves, using a stiff cantilever, for the locations with different amounts of phase shift on the worn surface of a physically-vapor-deposited TiN coating and showed that the influence of adhesion on the phase shift was negligible compared to the elastic modulus. We concluded, therefore, that the phase shift on a stiff surface was predominantly influenced by the elastic modulus and, conversely, the influence of adhesion was negligible, when a stiff cantilever was used. Therefore, the phase contrast images allow an estimation of relative stiffness of tribofilms as well as their inhomogeneity. However, the nature of this inhomogeneity can only be explained quantitatively with the help of additional information supplied from other analyses, such as dynamic spectroscopy in AFM, and chemical analyses such as Raman spectroscopy, AES and SIMS.

Diamond-like-carbon (DLC) coatings have received considerable attention due to their excellent chemical inertness, high wear resistance and a low friction coefficient and therefore they have successfully been applied in various applications. Tribological behavior of DLC coatings has been widely reported by numerous investigators. A study of worn surfaces of DLC coatings provides valuable information for assessing wear mechanisms involved in the sliding system. The wear mechanisms reported include formation of graphitic tribofilm on the contact surface of DLC coatings [17–19], degradation of mechanical properties (elastic modulus and hardness) without microstructural change in the bond structure of the DLC coating [20], material transfer from the film to the mating material or forming a layer of compact wear particles [21]. A better understanding of the nature of the tribofilms formed on the worn surfaces of the DLC coating and wear mechanisms can be achieved from the results of the phase contrast images and other chemical analyses. In the present investigation we demonstrated the significance of phase shift information of the AFM in the evaluation of DLC coating worn surfaces.

2. Experimental details

The DLC coating used for this study was deposited using an unfiltered pulsed vacuum arc deposition system with a pulse frequency of 20 Hz. The flat chromium–steel substrate (hardness ∼60 HRc) was polished to an average roughness of 0.135 µm (Ra) followed by an ultrasonic cleaning in an alkali water solution. The sample was sputter-cleaned prior to deposition using an Ar ion beam from a broad-beam ion source. A thin titanium nitride intermediate layer was deposited on the substrate to improve adhesion using a metal plasma source from a continuous current arc device at a negative bias of 1000 V. The pressure for DLC deposition was 7×10^{-3} Pa and the bias voltage was −500 V. The

temperature of the substrates during ionic bombardment and during deposition was around 473 K. The deposition time was 15 min. The thickness of DLC coating was 1.4 µm as measured by the α-step profilometer (Tencor© P1 Long Scan Profiler). The DLC coating hardness, measured using a microhardness system (PMT-3) with a load of 100 g, was approximately 65 GPa.

Dry oscillating wear tests were conducted at room temperature in a laboratory environment using a ball-on-plate tester. The balls were 3 mm diameter 52,100 steel ball. The upper ball specimen was reciprocating with a velocity of 0.01 m/s against the stationary DLC-coated flat specimen for 2×10^3 cycle. The applied load was 2.5 N.

Measurements of topography and phase shift were carried out using an AFM constructed in our collaborated laboratory. The oscillation of the probe was detected using an optical fiber interferometer. The probe was fabricated from a tungsten wire (100 µm diameter) by electrochemical etching. The following parameters were used for the tungsten probe installed in the AFM, $R = 100$ nm (measured using the standard test sample TGT01 supplied by NT-MDT), $\omega_0 = 44.9$ kHz, $Q_0 = 166$, $k_0 = 380$ N/m (calculated based on the geometry of the cantilever [22]). The mode of operation was tapping mode. The scanning parameters employed were $r_{sp} = 0.5$, $A_0 = 20$ nm and $A_{sp} = 10$ nm. We used a stiff cantilever for characterizing the hard sample. As described in Section 1, this tapping system will be sensitive to the stiffness of the sample surface and the influence of adhesion will not be significant. Therefore, it is plausible to say that, in this investigation, the relative variation of stiffness of the surface in the scan region can be identified from the phase contrast images.

To characterize the microstructure of the surface prior to and after the wear test, Raman spectra were measured with a T64000 micro-Raman spectrometer at room temperature. An Ar-ion laser, with a wavelength of 514.5 nm, was used. The physical and elemental characteristics of the surface were also investigated by PHI-670 Auger electron microscopy (AES) and PHI-7200 TOF-SIMS secondary ion mass spectrometry (SIMS). AES analysis was performed using a field emission gun with an accelerating voltage of 10 kV and a current of 0.0243 µA. The base pressure in the analysis chamber was 10^{-10} Torr. SIMS analysis was performed using a Ga ion gun with an accelerating voltage of 25 keV and a time-of-flight (TOF) mass analyzer.

3. Results and discussion

Fig. 1 shows the coefficient of friction as a function of sliding cycle. It showed a gradual decrease of friction coefficient until the test was terminated, indicating that the steady-state was not achieved during the test period. After 2000 cycles, the wear scar diameter of the mating steel ball was about 620 µm. The surface profile measurement of the wear track of the DLC coating using the α-step profiler is shown in
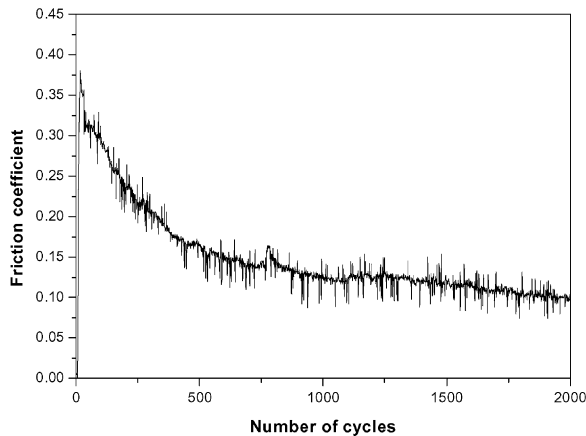
Fig. 1. Friction coefficient as a function of sliding cycle.

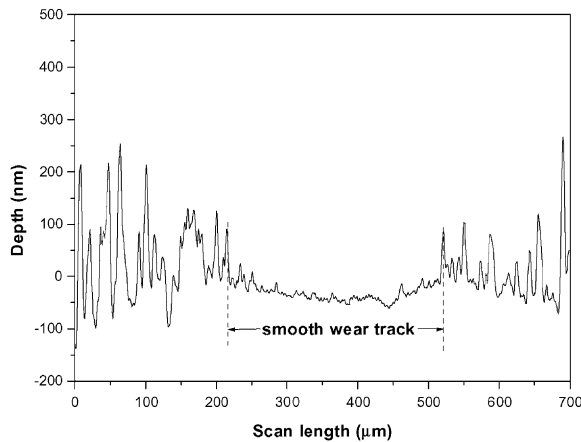Fig. 3. Division of friction contact zones for AFM measurement.

Fig. 2. Surface profile of the wear track perpendicular to the oscillating direction measured by the α-step profiler.

Fig. 2. It can be noted that the roughness decreased along the direction from the periphery to the center of the wear track where the surface was significantly smooth. The width of this smooth region was around 300 μm, which was much smaller than the wear scar diameter formed on the steel ball slider. The wear depth at the center of the wear track appeared to be <100 nm. The inspection of the worn surface by optical microscopy and SEM showed merely smoothening of the DLC layer. Therefore, the wear track was not discernable by optical microscopy and SEM. The surfaces before and after the friction contact were studied with an AFM. As the surface morphology and the roughness of the worn surface were in general inhomogeneous, they might vary depending on the locations relative to the center of the wear track. The sample surface was divided into four zones A, B, C and D, according to the distance from the center of the wear track (Fig. 3). The representative topography and phase contrast images of the unworn DLC coating surface (zone A) are displayed in Fig. 4. The phase contrast image of the unworn surface 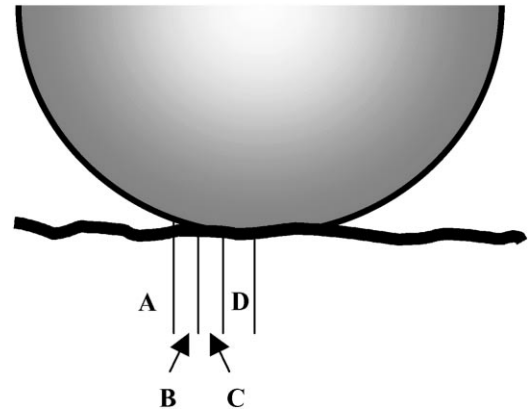revealed that the unfiltered pulsed vacuum arc deposition technique used in this investigation produced elliptical clusters, with <800 nm in length, which oriented to a certain direction. These DLC clusters formed individual asperities on the surface, encircled by cluster boundaries that appeared as a paving-stone-like pattern in the topography image. Each cluster was more clearly identified in the phase contrast image as shown in Fig. 4(b). Significant difference in stiffness between the clusters and their boundaries allowed the real cluster structures to appear in the phase contrast image. As the cluster boundaries were less stiff than the DLC clusters, they were represented as dark grey scale values in the phase contrast images, in contrast to the clusters shown with bright grey scale values. It can be also noted that the phase contrast images clearly revealed the structure of the clusters as compared to the topography images.

The topography and phase contrast images of the central zone of the wear track (zone D) is shown in Fig. 5. It revealed that the surface texture and the phase contrast image of the worn surface of the DLC coating were markedly different from the original surface. The clusters were not visible in the topography image Fig. 5(a) due to the surface films covering the coating surface. However, the phase contrast image (b) revealed the cluster structure underneath the films, indicating that the films were so thin that the probe tip–sample interaction was strongly influenced by the underlying DLC coating structure. There were many patches of relatively thick surface films deposited on the DLC clusters. It should be noted that considerable areas in the images were filled with very dark grey scale values and the rest with medium grey scale values. Both regions indicated the presence of materials with low stiffness (elastic modulus) but the dark grey regions exhibited relatively lower stiffness than the medium grey regions.

The images in Fig. 6 show the boundary region of the wear track (the zones B and C). The arrow in Fig. 6(a) denotes the oscillating direction of the counterface steel ball. The transition from the zones B to C was characterized by a sharp alteration in grey level from bright to dark grey scale values in the phase contrast image. The regions represented
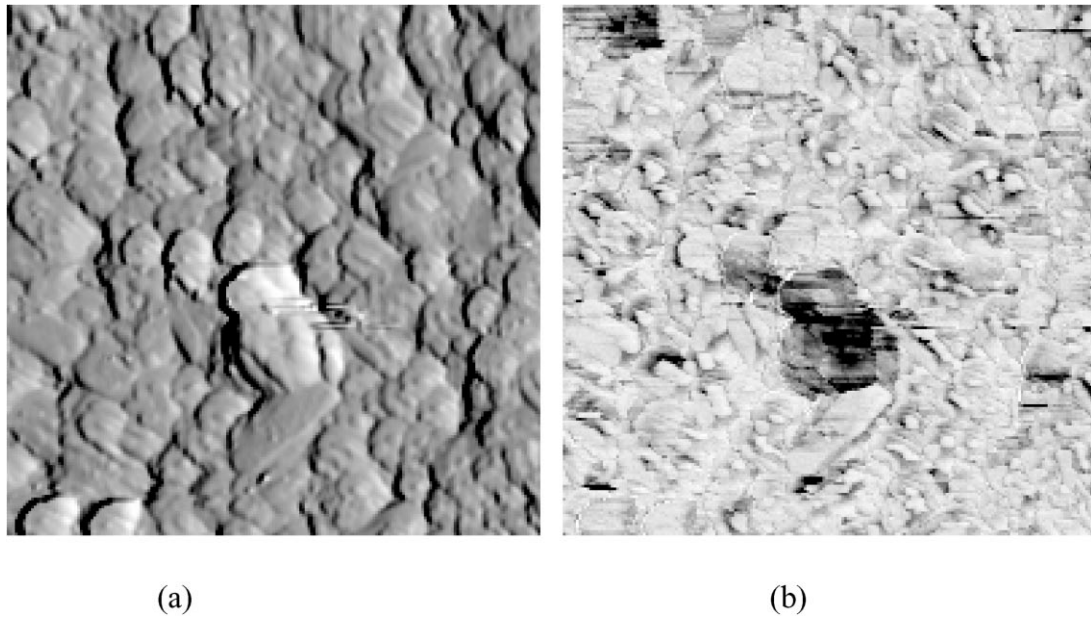
Fig. 4. AFM images of the unworn DLC film surface (zone A): (a) topography image ($R_q = 69.4$ nm, $h_{max} = 458.4$ nm); and (b) phase contrast image ($\Delta\Phi_{max} = 47.2°$) (scan size $= 10.7\,\mu$m $\times$ 10.7 μm).

as bright grey scale values corresponded to the zone B, not the original surface (zone A), as confirmed by the size and shape of the clusters. The average size of the clusters in the zone B was about twice bigger than that in the zone A, and the asperities were comparatively flattened. The difference in the cluster morphology between the zones B and C was not noticeable. However, the phase contrast in the zone C was smaller than the zone B. The line profiles of topography

and phase angle along the diagonal line, marked in Fig. 6(a) and (b), revealed that the surface roughness and the phase angle significantly decreased in the zone C (Fig. 6(c)). This roughness reduction was well correlated with the decrease of stiffness. Besides, the asperities in the zone C had a smaller slope (note the decrease of local tilt angle in Table 1). Above observations indicate that the dark sites in the phase contrast image can be attributed to tribofilms
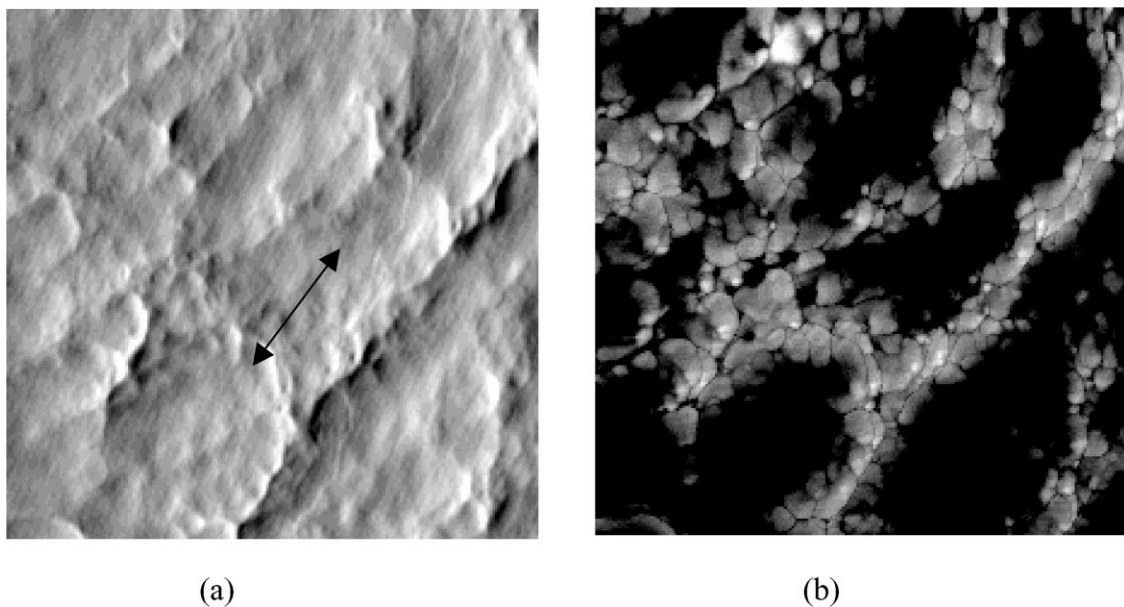

Fig. 5. AFM images of the worn surface (zone D): (a) topography image ($R_q = 13.8$ nm, $h_{max} = 92.2$ nm); and (b) phase contrast image ($\Delta\Phi_{max} = 24.0°$) (scan size $= 10.8\,\mu$m $\times$ 10.8 μm). The arrow shows the direction of oscillation of the counterface steel ball.
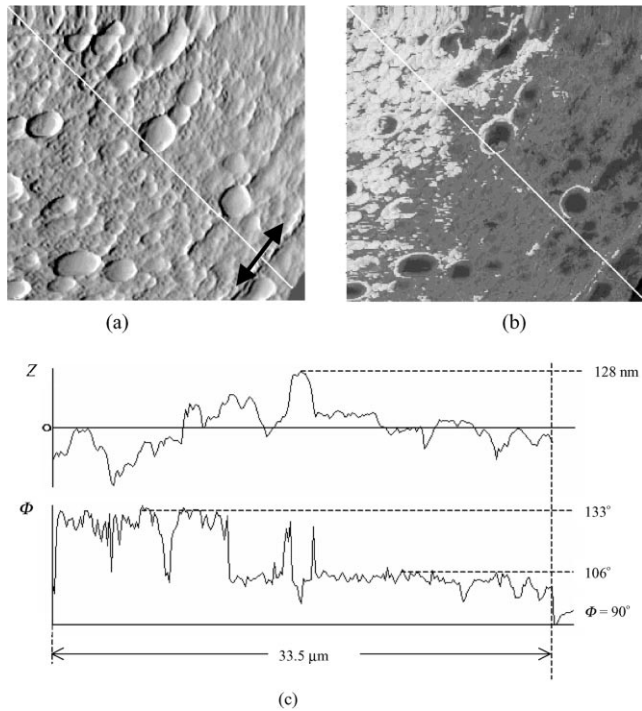
(a) (b)

(c)

Fig. 6. AFM images of the boundary of the wear track (zones B and C): (a) topography image (R_q = 64.9 nm, h_{max} = 230.7 nm); (b) phase contrast image ($\Delta\Phi_{max}$ = 37.1°) (scan size = 24.9 μm × 24.9 μm); and (c) variation of height (Z) and phase (Φ) along the diagonal line marked in (a) and (b), respectively.

which have lower elastic modulus than the original DLC coating. Furthermore, by comparing the local profile of topography with that of the phase angle, it was confirmed that the variation of the asperity height in topography image corresponded to the variation of the grey level in the phase contrast image that characterized the thickness of the tribofilms. A more detail analysis of the transition zone is given in Fig. 7. The topography image (a) clearly indicated

Table 1
Parameters for the asperities in the defined zones of the wear track on the DLC coating

Zone	R_q (nm)	α_{mid} (°)	α (°)	S (μm)	ζ
A (unworn surface)	52.0	16.6	10.8	0.74	0.3
B	21.1	4.9	2.2	1.30	0.4
C	16.1	3.3	1.8	1.20	0.4
D	14.3	2.0	1.2	0.55	0.5

the presence of the surface films. The height difference between the films and the adjacent areas, that showed different grey scale values in the phase contrast image (b), was carefully measured using the topography information and was assumed as the thickness of the corresponding films. The approximate thickness of these films at various locations was in the range 5–17 nm. Fig. 7(b) implied that the dark grey sites were related to the regions of asperity contact and were attributed to the tribofilms that were less stiff than the initial DLC material: the darker the grey scale values, the greater the thickness of the tribofilm. It should also be noted that the large clusters marked as A, B and C in the topography image, which were topographically higher than other clusters in the scan region, experienced more intense tribochemical reaction than the surrounding regions as they were under higher contact pressure and presumably under higher temperature due to frictional heat. The films deposited on these clusters showed much darker grey scale values in the phase contrast image, indicating that these films had much lower elastic modulus than the medium grey regions.

A three-dimensional simulation of the real contact area was performed to visualize the contact pressure distribution at real contact areas. We considered the force of interaction between the worn DLC coating surface and an approaching steel counterbody, which was assumed to be ideally flat within the region of the nominal contact. The topography data given in Fig. 8(a), obtained from the central region of the wear track, was used for the rough DLC coating surface.
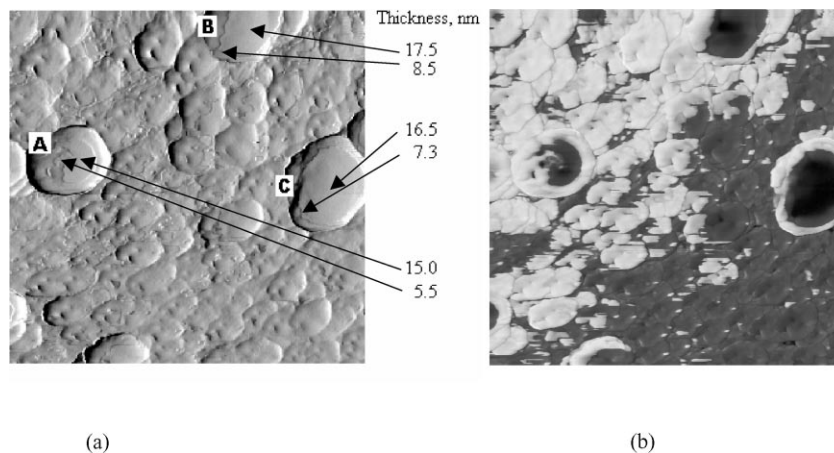

(a) (b)

Fig. 7. AFM images of the boundary of the wear track (zones B and C) and thickness of the tribofilm: (a) topography image (R_q = 33.7 nm, h_{max} = 157.5 nm); and (b) phase contrast image ($\Delta\Phi_{max}$ = 49.1°) (scan size = 13 μm × 13 μm).
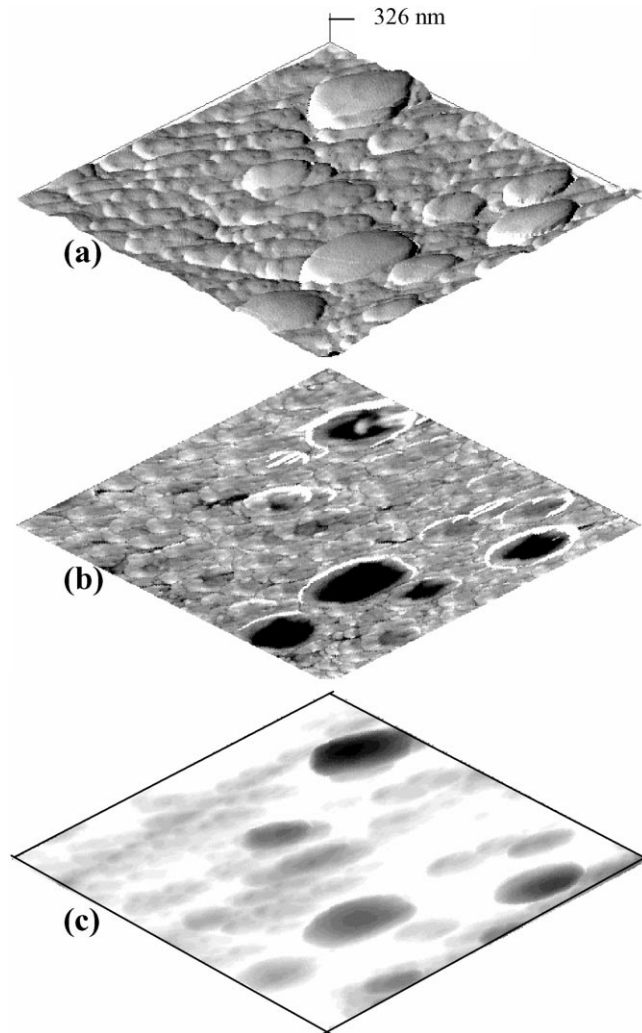
Fig. 8. (a) Topography image ($R_q = 43.9$ nm, $h_{max} = 147.7$ nm); (b) phase contrast image ($\Delta\phi_{max} = 48.8°$) (scan size = 12.4 μm × 12.4 μm); and (c) simulated real contact pressure (average contact pressure 525 MPa).

Fig. 9. Histograms of the phase shift: (a) zone A; (b) boundary between the zones B and C; and (c) zone D.

The simple Winkler model was employed to describe the elastic deformation where the contact surfaces were modeled as a set of elastic bars or springs, not connected laterally with each other. The details of this simulation procedure can be seen elsewhere [23–25]. The result of the simulation, shown in (c), revealed that there was an excellent agreement between the phase contrast image (b) and the simulated contact pressure distribution. The darker regions corresponded to the regions with higher contact pressure, confirming the formation of the thicker tribofilms at the regions of maximum force interaction between the two surfaces.

The histograms in Fig. 9 show distributions of phase angle for the phase contrast images in the Figs. 4(b), 5(b) and 6(b), respectively. The histograms revealed three different features. The location of the peak in the right in Fig. 9(b) coincided with that corresponded to the unworn DLC surface (Fig. 9(a)). It is conceivable that the surface topography at the wear track boundary was modified but the local
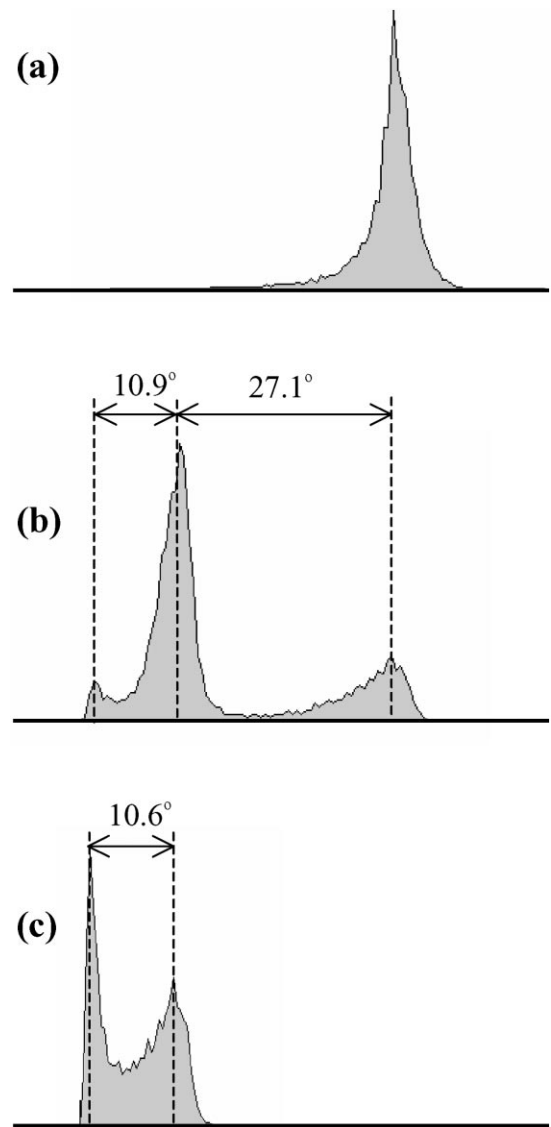
micromechanical properties of this region remained unaffected during the sliding contact. Two other peaks in the left in (b), significantly shifted from the peak related to the unworn DLC surface, reflected medium and dark grey scale values attributed to the tribofilms (Fig. 6(b)). The difference in the micromechanical properties between the original DLC coating and the tribofilms caused the phase shift of the oscillating cantilever as much as 27–30°. The difference of the phase shift between the medium grey and dark grey regions of the tribofilms was 10–11°.

Table 1 shows the comparison of quantitative roughness parameters for the zones A–D. The parameters listed in the table are, RMS profile deviation (R_q), mean local tilt angle (α_{mid}), most probable value of the surface tilt angle α, average size of the cluster (S), and anisotropy coefficient (ζ) (for isotropic surface, $\zeta = 1$). By comparing the roughness

of the unworn surface (zone A) and central part of the wear track (zone D), one can notice that a considerable smoothening of the surface occurred. The clusters in the worn surface became smaller and were not higher than 30 nm. Despite of the microgrooves, R_q of the central part of the wear track was more than three times smaller than that of the unworn surface. The greater value of the parameter ζ, after sliding contact, indicates that the surface became more isotropic. The smaller values of α_{mid} and α implied that the slope of asperities reduced, i.e. the asperities had a greater radius of curvature.

Fig. 10 shows the typical microlaser Raman spectra of the DLC coating prior to and after the wear test. The Raman spectrum obtained form the original surface revealed only a broad peak at 1550 cm^{-1} that corresponded to an amorphous hydrocarbon with a high sp^2/sp^3 ratio [26]. On the other hand, graphitic material was evident in the spectrum measured for the debris attached on the wear track. The peaks at 1350 and 1580 cm^{-1} corresponded to the D and G peaks of crystalline graphite, respectively [26]. Another peak at 662 cm^{-1} was attributed to iron oxide (α-Fe$_2$O$_3$) [27]. One can note that the Raman spectrum of the worn surface did not apparently show any difference from that of the original surface. We assume that this was due to the negligible contribution of the tribofilms to the Raman scattering comparing with that of the bulk coating since the thickness of the tribofilms was much smaller than the penetration depth of Ar-ion laser, employed in this Raman spectroscopy. The analysis of the wear particle and asperities on the worn surface by AES (Fig. 11) showed that carbon was the most dominant element in the worn surface. The chemical composition of the irregular-shaped wear particle, marked as the rectangular area 1, was dominated by steel composition except the relatively high carbon content, implying that a tribochemical reaction took place on the contacting steel ball surface. The material transfer from the steel ball slider to the DLC coating was found to be insignificant. The SIMS analysis supported the above observation (Fig. 12). Figure (a) shows the total sum of the ions detected in the measured area whereas (b) only displays Fe ion. It is clear that the major
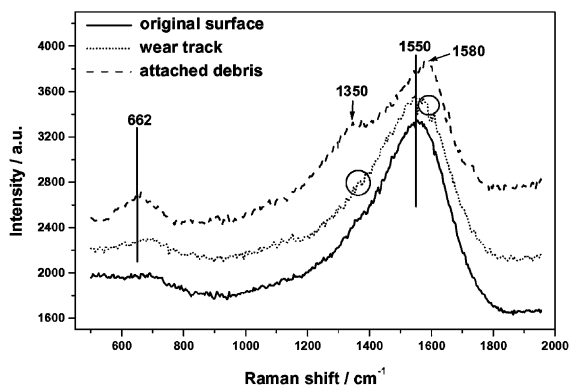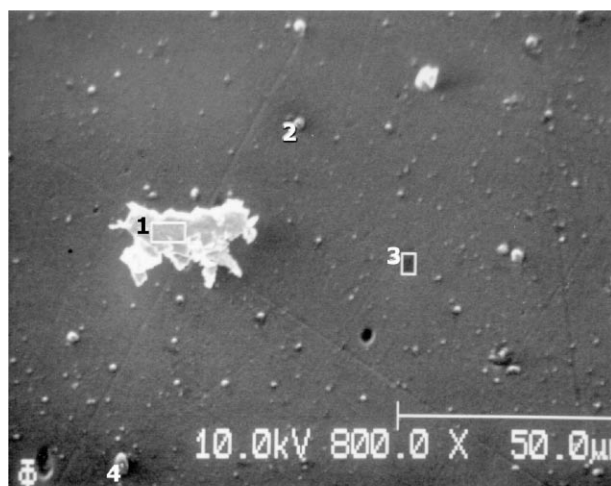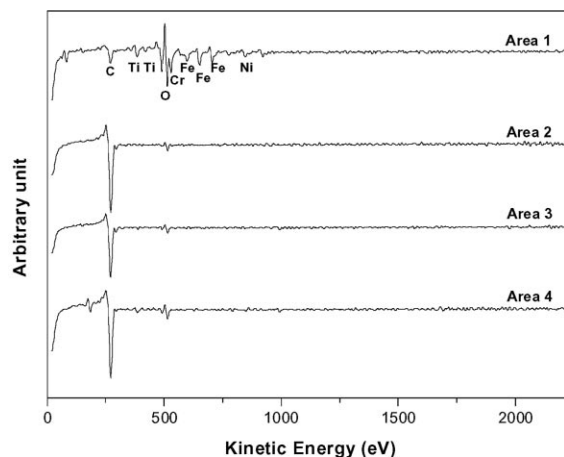

(a)

(b)

Fig. 11. (a) SEM image; and (b) AES spectra of the wear track.

contribution to the total sum of the ions was carbon ion as the intensity of Fe ion in (b) was very low. It is obvious, therefore, that the tribofilms were composed dominantly of carbon. These observations suggest that the tribofilms may be mostly composed of graphite formed by a tribochemical reaction.

Comparison of the results obtained by atomic force microscopy with those of micro-Raman, AES and SIMS analyses led to a speculation that the tribolfilms, composed almost of carbon element, may be graphite films or films mainly possessing graphitic property. This is probably the main reason of the significant (more than three times) decrease of the friction coefficient observed in this work. The tribofilms formed on the worn surface protected the DLC coating surface inspite of their nanometer-scale thickness. The high contact pressure and temperature exerted to the contact

Fig. 10. Micro-Raman spectra of the DLC coating prior to and after the wear test, and the debris attached on the worn surface.
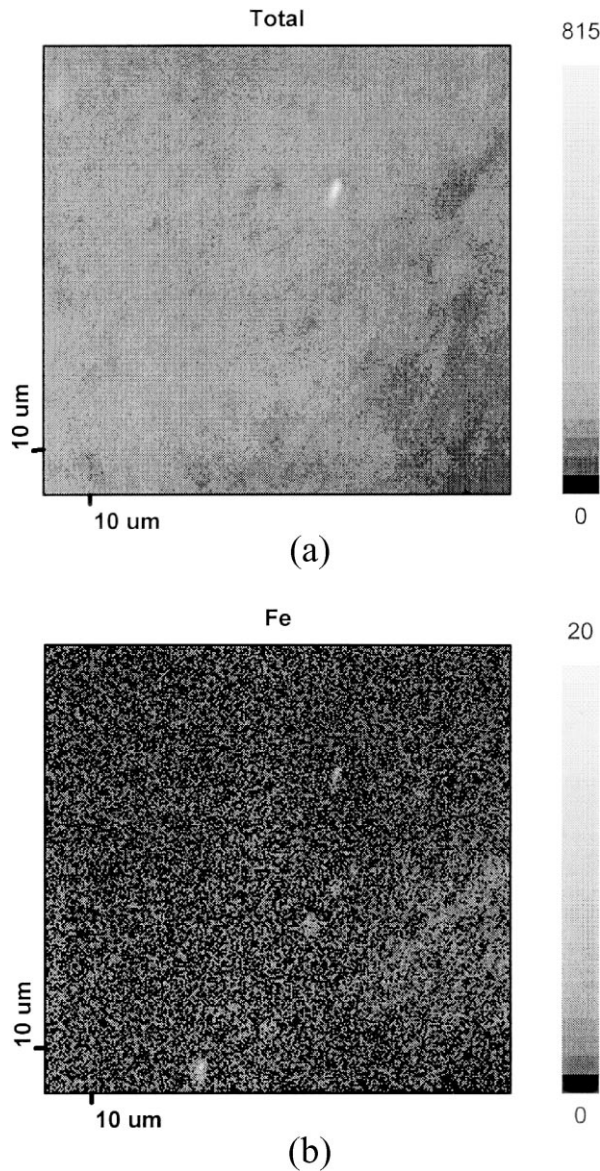
Fig. 12. SIMS analysis results of the wear track: (a) total ions intensity map; and (b) Fe ion intensity map.

surface can initiate the transition of the diamond-like structure to the graphite-like structure. The latter has lower elastic modulus than the former. Therefore, a significant decrease of the phase shift occurred when the probe tip traveled over these films. The films had the greatest thickness at the asperity summits where the local contact pressure was high and temperature flash was the most probable. It is likely that the transition from amorphous carbon to polycrystalline graphite dominantly occurred at the high asperity peaks.

4. Conclusions

This investigation demonstrated the high efficiency of combined analysis of topography and phase contrast images obtained with a tapping mode AFM for characterizing the DLC coating worn surfaces. The phase contrast images allow a qualitative estimation of relative stiffness (elastic modulus) of the sample surface. Particularly, phase contrast images are capable of revealing the formation of tribofilms. Use of this technique for investigating the wear surfaces of DLC coatings has led to the following conclusions.

1. Study of the worn surface using the described technique revealed significant inhomogeneity of the wear track across the sliding direction.
2. Thin tribofilms having elastic modulus much lower then that of the DLC coating was formed on the DLC coating surface. Formation of these tribofilms may be related to the graphitization process of amorphous carbon by a tribochemical reaction.
3. The comparison of the simulated contact pressure distribution and the phase contrast images revealed the localization of the tribofilms at the real contact regions and their increased thickness on the higher asperity peaks.
4. The phase contrast imaging in atomic force microscopy showed a promise as an effective tool for better understanding of micromechanical properties of worn surfaces. It may provide insight into the formation of surface films and the influence of its microstructure on friction and wear process.

Acknowledgements

References

[1] B. Bhushan, Handbook or Micro- and Nanotribology, CRC Press, New York, 1995.
[2] O. Marti, Physica. Scripta. T49 (1993) 599–604.
[3] M. Bingelli, C.M. Mate, Appl. Phys. Lett. 65 (1994) 415–417.
[4] B. Anczukowski, D. Krüger, H. Fuchs, Phys. Rev. B 53 (1996) 15485–15488.
[5] R.G. Winkler, J.P. Spatz, S. Sheiko, M. Moller, P. Reineker, O. Marti, Phys. Rev. B54 (1996) 8908–8912.
[6] S.N. Magonov, V. Elings, M.-H. Whangbo, Surf. Sci. Lett. 375 (1997) L385–391.
[7] J. Tamayo, R. García, Appl. Phys. Lett. 71 (1997) 2394–2396.
[8] H.G. Hansma, K.J. Kim, D.E. Laney, J. Str. Biol. 119 (1997) 99–108.
[9] I. Schmitz, M. Schreiner, G. Friedbacher, M. Grasserbauer, Appl. Surf. Sci. 115 (1997) 190–198.
[10] G. Haugstadt, R.R. Jones, Ultramicroscopy 76 (1999) 77–86.
[11] M.W. Nelson, P.G. Schroeder, R. Schlaf, B.A. Parkinson, J. Vac. Sci. Technol. B 17 (1999) 1354–1360.
[12] K.A. Ramirez-Aguilar, D.W. Lehmpuhl, A.E. Micchael, J.W. Birks, K.L. Rowlen, Ultramicroscopy 77 (1999) 187–194.
[13] L. Wang, Appl. Phys. Lett. 73 (1998) 3781–3783.
[14] H.-S. Ahn, S.A. Chizhik, Appl. Phys. Lett., 2001, submitted.
[15] H.-S. Ahn, S.A. Chizhik, A.M. Dubravin, Friction and Wear 20 1999, 613–622 (in Russian).
[16] H.-S. Ahn, S.A. Chizhik, I. Luzinov, KSTLE Int. J., 2000, 69–75.
[17] T.A. Yeh, C.-L. Lin, J.M. Sivertsen, J.H. Judy, G.-L. Chen, IEEE Trans. Mag. 29 (1993) 3939–3941.

[18] Y. Liu, A. Erdermir, E.I. Meletis, Surf. Coat. Technol. 82 (1996) 48–56.

[19] J.F. Zhao, Z.H. Liu, J. McLaughlin, Thin Solid Films 357 (1999) 159–165.

[20] J. Koskinen, D. Schneider, H. Ronkainen, T. Mukkonen, S. Varjus, P. Burck, K. Holmberg, H.J. Scheibe, Surf. Coat. Technol. 108/109 (1998) 385–390.

[21] J. Jiang, R.D. Arnell, J. Tong, Wear 214 (1998) 14–22.

[22] D. Sarid, Scanning Force Microscopy, Oxford University Press, New York, 1994.

[23] S.A. Chizhik, V.V. Gorbunov, N.K. Myshkin, Prec. Eng. 17 (1995) 186–191.

[24] S.A. Chizhik, S.A.V. Goldade, N.K. Myshkin, Int. J. Mach. Tools Manufact. 38 (1998) 495–502.

[25] S.A. Chizhik, N.B. Gaiduk, N.K. Myshkin, Metrology and properties of engineering surfaces, in: Proceedings of the Eighth International conference, UK, April 2000, pp. 65–69.

[26] D.S. Knight, W.B. White, J. Mater. Res. 4 (1989) 385–393.

[27] S. Wang, W. Wang, W. Wang, Z. Jiao, J. Liu, Y. Qian, Sens. Actuators B 69 (2000) 22–27.